Published online 21 February 2017

Nucleic Acids Research, 2017, Vol. 45, No. 10 ***6011–6022***
doi: 10.1093/nar/gkx134

Coordination among tertiary base pairs results in an efficient frameshift-stimulating RNA pseudoknot

Yu-Ting Chen[1,†], Kai-Chun Chang[1,†], Hao-Teng Hu[2], Yi-Lan Chen[3], You-Hsin Lin[1], Chiung-Fang Hsu[1], Cheng-Fu Chang[1], Kung-Yao Chang[2] and Jin-Der Wen[1,3,4,*]

[1]Institute of Molecular and Cellular Biology, National Taiwan University, Taipei 10617, Taiwan, [2]Institute of Biochemistry, National Chung-Hsing University, Taichung 40227, Taiwan, [3]Genome and Systems Biology Degree Program, National Taiwan University and Academia Sinica, Taipei 10617, Taiwan and [4]Department of Life Science, National Taiwan University, Taipei 10617, Taiwan

Received January 05, 2017; Revised February 14, 2017; Editorial Decision February 15, 2017; Accepted February 17, 2017

ABSTRACT

Frameshifting is an essential process that regulates protein synthesis in many viruses. The ribosome may slip backward when encountering a frameshift motif on the messenger RNA, which usually contains a pseudoknot structure involving tertiary base pair interactions. Due to the lack of detailed molecular explanations, previous studies investigating which features of the pseudoknot are important to stimulate frameshifting have presented diverse conclusions. Here we constructed a bimolecular pseudoknot to dissect the interior tertiary base pairs and used single-molecule approaches to assess the structure targeted by ribosomes. We found that the first ribosome target stem was resistant to unwinding when the neighboring loop was confined along the stem; such constrained conformation was dependent on the presence of consecutive adenosines in this loop. Mutations that disrupted the distal base triples abolished all remaining tertiary base pairs. Changes in frameshifting efficiency correlated with the stem unwinding resistance. Our results demonstrate that various tertiary base pairs are coordinated inside a highly efficient frameshift-stimulating RNA pseudoknot and suggest a mechanism by which mechanical resistance of the pseudoknot may persistently act on translocating ribosomes.

INTRODUCTION

Translation is the process of protein synthesis catalyzed by ribosomes. The ribosome reads consecutive codons along the messenger RNA (mRNA) until reaching a stop codon, which marks the end of translation. A codon consists of three nucleotides, and thus there are three possible reading frames for a given mRNA. Under some circumstances, the ribosome may move from one frame to another during translation by skipping or rereading a nucleotide of the mRNA, resulting in +1 or −1 frameshifting, respectively. Minus-one frameshifting is commonly used to regulate the relative expression levels of two proteins in many viruses and bacteria, where specific mRNA sequences and structures are devised to stimulate frameshifting with a certain efficiency, a process termed programmed ribosomal frameshifting (PRF) (1–4).

In general, −1 PRF occurs at a heptanucleotide sequence (i.e. a slippery sequence) with a pattern of XXXYYYZ, where X can be any nucleotide, Y can be A or U, and Z is usually not G (5,6). The pattern minimizes mismatches between the codons and transfer RNA (tRNA) anticodons after shifting (X-XXY-YYZ for the 0 frame and XXX-YYY-Z for the −1 frame). The slippery sequence is followed by an RNA structure, which is critical for frameshift stimulation (7). Pseudoknot structures are common stimulators found in many viruses, including coronaviruses, retroviruses and luteoviruses (8,9). The human immunodeficiency virus type 1 (HIV-1) instead uses a hairpin as a stimulator at the *gag-pol* junction (10). Several models have been proposed to explain how various RNA structures function during this process (9,11–17). Based on the HIV-1 system, it was suggested that the frameshifting efficiency was correlated with the thermodynamic stability of the hairpins (15). However, by systematically changing the HIV-1 hairpin sequence, a recent study revealed that the frameshifting efficiency correlated with the local stability of the first 3–4 base pairs (bp) in the hairpin stem, rather than the overall structure (16). Given that the mRNA entrance site of the prokaryotic ribosome possesses helicase activity (18) and that the ribosome unwinds an mRNA hairpin during translation 3 bp at a time (19,20), the first few base pairs of the stem ap-

*To whom correspondence should be addressed. Tel: +886 2 3366 2486; Fax: +886 2 3366 2478; Email: jdwen@ntu.edu.tw
†These authors contributed equally to the paper as first authors.
Present address: You-Hsin Lin, Department of Cell Pharmacology, Nagoya University Graduate School of Medicine, Nagoya 466-8550, Japan.

pear to play a far more important role than the whole RNA hairpin in stimulating frameshifting. However, the situation becomes more complicated when the frameshift-stimulating structure is a pseudoknot that involves tertiary base pair interactions.

From a study using cryo-electron microscopy to investigate the ribosome–mRNA complex that was stalled in the process of −1 frameshifting, the mRNA entrance site of the ribosome was shown to be in contact with the RNA pseudoknot, which was modified from the infectious bronchitis virus (IBV) (11). When the ribosome approaches an mRNA pseudoknot, stem S1/loop L2 of the structure is likely to be the first target for the ribosomal helicase (21) (see Figure 1A for nomenclature). Chemical probing analysis of the beet western yellows virus (BWYV) pseudoknot within a pre-translocation ribosome has revealed a ribosome-dependent protection pattern change of the nucleotides spanning the S1/L2 junction (22). Of several known frameshift-stimulating pseudoknots, including those from BWYV and simian retrovirus type-1 (SRV-1), stem S1 is G/C-rich and 5–6 bp long, and most nucleotides in loop L2 are adenosines appearing in stretches (9,23–29) (Supplementary Figure S1). Base triple interactions between stem S1 and the adenosines of loop L2, which span the minor groove of stem S1, are commonly found in these pseudoknots. Frameshifting efficiency was reduced to ∼10% of the original level when the loop nucleotides of the SRV-1 pseudoknot were replaced by pyrimidines (30). Likewise, the adenosine stretch is absent from a non-frameshift-stimulating pseudoknot derived from the bacteriophage T2 (29,31). The tertiary base pairs involving loop L2 may locally increase the mechanical, as well as thermal, stability of stem S1 and thus provide enhanced resistance to helix unwinding for the ribosomal helicase during the process of frameshifting.

The tertiary base pairs inside an RNA pseudoknot can be modulated to change its mechanical stability, which then can be measured using optical tweezers (32). In this way, Chen *et al.* used DU177, a pseudoknot derived from the human telomerase RNA (33,34), as a model system to explore how the mechanical stability of pseudoknots affect frameshifting (13). Like the other frameshift-stimulating pseudoknots mentioned above, loop L2 of DU177 contains a stretch of adenosines spanning the minor groove of stem S1, where two base triples (A•U*A and C•G*A) are formed (see Figure 1A) (33,35). In addition, three identical major groove base triples (U•A*U) and a Hoogsteen A*U base pair appear in S2/L1 and at the junction of S1/S2, respectively. Mutations that block the formation of some of the base triples result in the decrease of not only the unfolding force (the force required to unfold the structure) but also the frameshifting efficiency (13). Disrupting all five of the base triples results in the DU177 mutant completely losing its capability to stimulate frameshifting, though the mutant still folds into a pseudoknot conformation (36). A recent study using the SRV-1 pseudoknot and its base triple mutants also yielded a similar conclusion (17). However, the correlation in unfolding force versus frameshifting efficiency was not observed when comparisons were made between pseudoknots derived from a variety of viruses of different sizes and folding topology (14). Most of the pseudoknots tended, with various degrees, to fold into alternative structures and this tendency showed a greater correlation with the frameshifting efficiency than unfolding force (14,37). Thus, features other than the overall mechanical stability of a pseudoknot remain to be uncovered to understand the molecular mechanism of ribosomal frameshifting in more detail.

In this study, we aimed to investigate the local structure of a pseudoknot first targeted by translocating ribosomes, i.e. the region involving stem S1 and loop L2. We used bimolecular pseudoknots to mimic the DU177 pseudoknot conformation (36), such that the mechanical strength of stem S1 (under the influence of loop L2), instead of the whole pseudoknot, could be measured using optical tweezers. We found that the helix unwinding resistance was enhanced additively and sequentially by the major groove base triples, minor groove base triples, and then the adenosine stretch. Single-molecule Förster Resonance Energy Transfer (sm-FRET) (38) experiments further suggested that the adenosine stretch was confined along the minor groove of the helix to prevent it from twisting. Both the helix unwinding resistance and the frameshifting efficiency decreased when the adenosine stretch was mutated. By dissecting the pseudoknot's tertiary base pair interactions, our results provide great insight into the structural dynamics of a –1 frameshift stimulator.

MATERIALS AND METHODS

In vitro translation assays for frameshifting

DNA oligomers containing the slippery (TTTAAAC), linker (GGGTT) and stimulatory sequences (DU177 or hp1) were chemically synthesized and inserted into the reporter p2luc plasmid (39), a gift from Prof. John Atkins, between the SalI and BamHI restriction sites. The 0 frame and −1 frame stop codons on the constructs correspond to protein products with molecular weights of 37.4 and ∼100 kDa, respectively. A modified version of DU177, named DU177ps, was constructed by introducing a −1 frame stop codon before the BamHI site to generate a smaller product (40.1 kDa) to minimize potential ribosome fall-off during translation. The UUC mutant (UUCps) was modified from DU177ps using site-specific mutagenesis. The mRNA was prepared by transcribing the DNA constructs using T7 RNA polymerase, followed by a 5′-capping reaction using m7G(5′)ppp(5′)G RNA Cap Structure Analog (NEB). *In vitro* translation was carried out in the reticulocyte lysate system (Ambion). For each reaction, a total volume of 5 μl containing 100 ng of capped mRNA, 2.5 μl of reticulocyte lysate and 1 μCi of ^{35}S-labeled methionine (NEN) was incubated at 30°C for 100 min. In the case of hp1 mRNA, various amounts of the specified RNA oligomers were also added for annealing. The reaction products were resolved on a 12% sodium dodecyl sulphate-polyacrylamide gel electrophoresis gel and visualized by autoradiography. The difference in methionine content of the proteins was corrected.

Sample preparation for optical tweezers experiments

DNA sequences for DU177 and related mutants were chemically synthesized and inserted into the pVE60hp plasmid

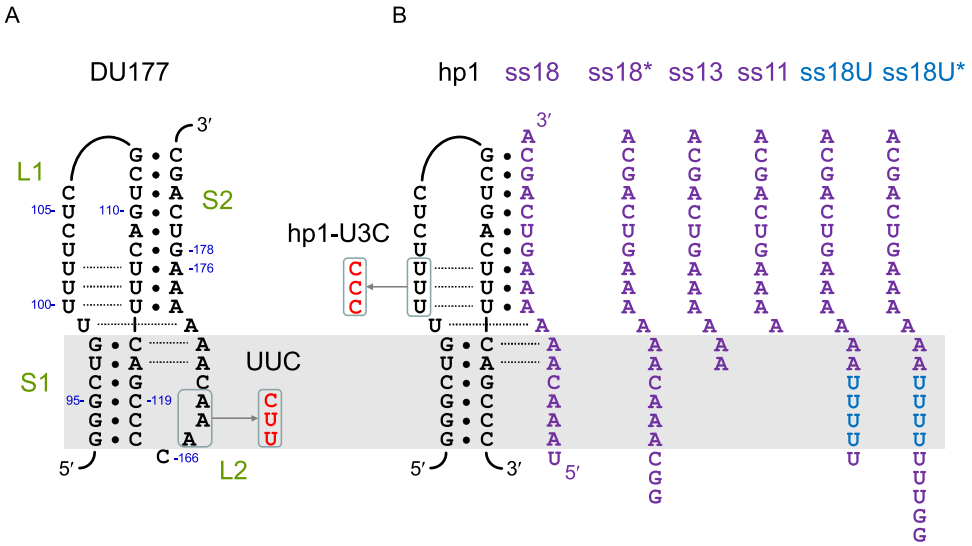

Figure 1. DU177 and the design of the bimolecular pseudoknots. (**A**) A schematic of the DU177 pseudoknot. Nucleotides involved in base triples or Hoogsteen base pairs are connected by dotted lines. The sequence change in the UUC mutant is indicated. (**B**) Schematics of the bimolecular pseudoknots derived from DU177. The sequence change in the mutant hairpin hp1-U3C is indicated. The series of RNA oligomers used for annealing are shown on the right. The gray shaded area highlights the corresponding stem S1 region for better comparison among various constructs. Both ss18* and ss18U* were made by *invitro* transcription, and thus contained two G's (from the promoter sequence) at the 5′ end. The others (ss11–ss18) were chemically synthesized.

(20) between the NdeI and BsrGI restriction sites. The resulting plasmids, containing a T7 promoter located ∼750 bp upstream from the insertion site, were cut at the BssSI site (∼900 bp downstream from the insertion site) and transcribed into RNA using the MEGAscript T7 Kit (Invitrogen). Two DNA handles were prepared using PCR, tag labelled, and then annealed to the RNA transcripts as described previously (40). In the finished RNA constructs, the 5′ handle was 737 bp long with a digoxigenin tag, and the 3′ handle was 917 bp long with a biotin tag. To make bimolecular pseudoknots, 2.5 nM of the handle-annealed hp1 construct were mixed with a 20-fold molar excess of chemically synthesized RNA oligomers (Thermo Scientific) and incubated at 37°C for 15 min.

Sample preparation for smFRET experiments

To make RNA samples for smFRET experiments, another parental vector, pT7SP6, was used for plasmid construction. pT7SP6 was created by inserting the SP6 promoter into pVE60hp between the XmaI and SpeI restriction sites, 718 bp downstream from the T7 promoter. Transcription from the SP6 promoter will bypass most of the 5′ handle sequence, which was not required for smFRET experiments. DNA sequences for hp1 and related constructs were chemically synthesized and cloned into pT7SP6 between SpeI and BsrGI. The constructed plasmids were cut at the BsrGI site and transcribed into RNA by using the MEGAscript SP6 Kit (Invitrogen).

Dye-labeled RNA oligomers were synthesized by Dharmacon, with Dy647 (acceptor) and Dy547 (donor) covalently linked to the 5′ and 3′ ends, respectively. Single-stranded DNAs (dna9–dna16) were synthesized (Life Technologies) with a $(dC)_{21}$ linker and a biotin tag on the 5′ end for immobilization.

Measurements using optical tweezers

The experimental setup for optical tweezers is illustrated in Supplementary Figure S2. Detailed procedures have been described previously (20,41). Briefly, the two ends of an RNA construct were attached to two 2.1 μm polystyrene beads coated with streptavidin and anti-digoxigenin antibodies, respectively. One bead was fixed on a micropipette and the other was trapped by laser beams. To pull the molecule, the trap was moved at a rate of 100 nm/s. The experiments were performed in a buffer containing 10 mM Tris–HCl (pH 7.0), 200 mM NaCl and 0.1 mM EDTA, unless otherwise noted. Data from optical tweezers were recorded at 1000 Hz and averaged to 100 Hz. Data analysis and worm-like chain modeling (42) for structural transitions were performed using custom-written MATLAB (MathWorks) programs as described previously (41).

Measurements of smFRET

smFRET measurements were performed using a home-built total internal reflection fluorescence (TIRF) microscope (IX71, Olympus) equipped with a 100× objective (UAPON 100XOTIRF, Olympus), a 532-nm laser (CL532-075-L, CrystaLaer) and an EMCCD (iXon DU-897D, Andor). Details of the microscope setup are described in Supplementary Methods.

Dye-labeled RNA complexes were immobilized on a slide surface, in a buffer containing 40 mM HEPES-KOH (pH 7.5), 70 mM NH_4Cl, 7 mM $Mg(OAc)_2$ and 1.7 mM Trolox (Sigma-Aldrich). To improve dye stability, the following oxygen scavenging system (43) was also included in the buffer: 2.6 mM protocatechuic acid (PCA; Sigma-Aldrich) and 48 nM protocatechuate 3,4-dioxygenase (PCD; Sigma-Aldrich). Fluorescence movies were recorded at 20 Hz using SMET, a LabView-based program package (44), and

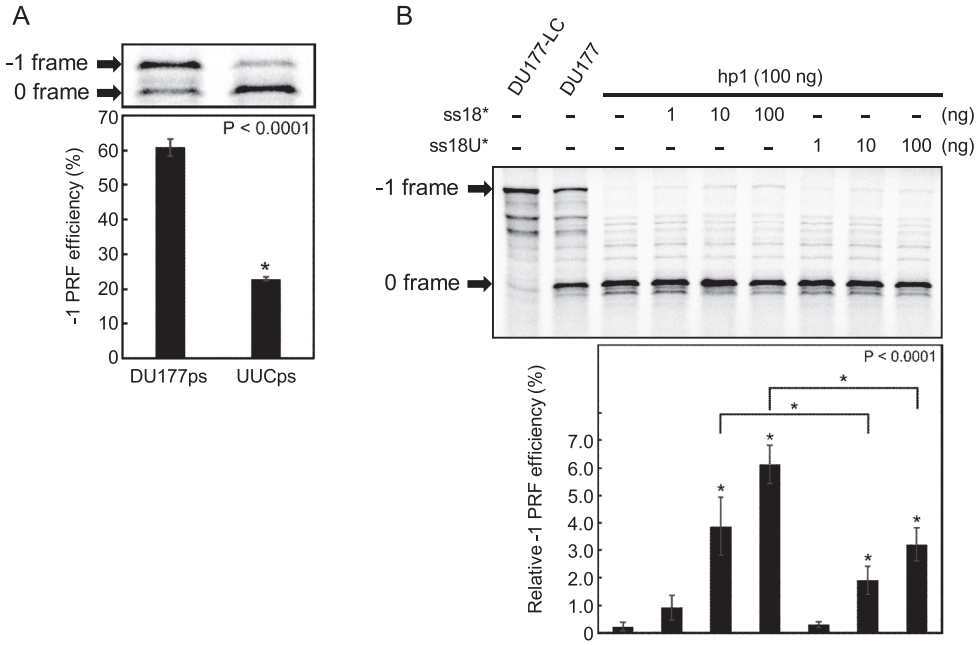

Figure 2. *Invitro* translation assays for frameshifting. Representative phosphor images are shown on top of each panel. The 0 and −1 frame protein products are indicated. Frameshifting efficiency statistics for each sample are shown at the bottom. (**A**) mRNA of DU177ps (lane 1) and UUCps (lane 2) containing the regular pseudoknots from DU177 and the UUC mutant, respectively. (**B**) mRNA containing the hairpin hp1 to form bimolecular pseudoknots in the absence (lane 3) or presence of indicated amounts of ss18* (lanes 4–6) and ss18U* (lanes 7–9). Lane 2, control mRNA containing the native DU177 instead of hp1. Frameshifting efficiency shown at the bottom is normalized to this sample. Lane 1, control mRNA as in lane 2 except for deletion of the slippery sequence to highlight the −1 frame protein product. Data from at least three independent experiments were averaged. Error bars show standard deviation. * indicates $P < 0.0001$ as determined by *t*-test. In panel B, comparisons are made with lane 3 or between indicated sample pairs.

processed by the IDL (Exelis) scripts released from Taekjip Ha's lab (https://cplc.illinois.edu/software). Time-evolved smFRET traces were analyzed by custom-written MATLAB programs. The first 10 data points from each trace were averaged and reported for FRET distribution.

RESULTS

Role of the loop L2 adenosine stretch

Six out of the eight nucleotides in loop L2 of DU177 are adenosines; three are involved in tertiary base pairs, whereas the other three (A167, A168 and A169) do not appear to form any hydrogen bonds with neighboring strands (33,35) (see Figure 1A). Replacing one or two of these unpaired A's with pyrimidines (C or U) decreased the frameshifting efficiency by 20–40% (36). When we changed all three to UUC and repeated the *in vitro* translation assay, a larger decrease of 62% in frameshifting efficiency [from 61 to 23%, Figure 2A; (61–23)/61 = 62.2%] was observed. Both the previous and current data indicate that, while not involved in base pairing, the adenosine stretch in loop L2 of the pseudoknot plays a critical role in frameshift stimulation.

Furthermore, we used optical tweezers (Supplementary Figure S2) to measure the unfolding force of the L2 mutant (referred to as UUC hereinafter) to determine if its mechanical stability was also weakened, as was observed for the base triple mutants (13). Figure 3A shows three typical force-extension curves obtained during the structural unfolding process of the original DU177. The results were generally similar to the previously reported data (13); DU177 can exist in the well-folded native pseudoknot (type I) or in a less stable intermediate that is lacking some of the tertiary base pairs (type II). During the force ramping process, the intermediate structure may first break into the constituent stem-loop hairpin (S1-L1) before being completely opened, as revealed by the two-step transitions in some of the force-extension curves (type III). Thus, the last transition of this type of unfolding pattern mostly corresponded to ripping of the S1-L1 hairpin [see (13) for more information regarding the folding/unfolding of DU177]. Figure 3B (top panel) shows more than 450 unfolding transitions for DU177, and the distribution of unfolding force is plotted in Figure 3C (top panel). The native pseudoknot required an average force of 42.3 pN for unfolding, well above that of all the intermediates (14.8 pN). A bipartite distribution of unfolding force was also observed for the UUC mutant (Figure 3B and C, bottom panels). Compared to DU177, the low-force peak (15.3 pN) was similar, while the high-force peak (39.1 pN) was slightly less by ∼8%. The minor reduction in pseudoknot unfolding force cannot fully explain the sizeable decrease in frameshifting efficiency (by 62%). Specifically, the three unpaired nucleotides (A167, A168 and A169) in loop L2 contributed modestly to the structural stability but significantly to the frameshift stimulation. In addition, only 16% of the strong stimulator DU177 folded into the native pseudoknot, as opposed to 89% for the weak stimulator UUC mutant (Figure 3C). These observations can be explained by dissecting and investigating the tertiary base pair interactions inside the pseudoknot (see below).

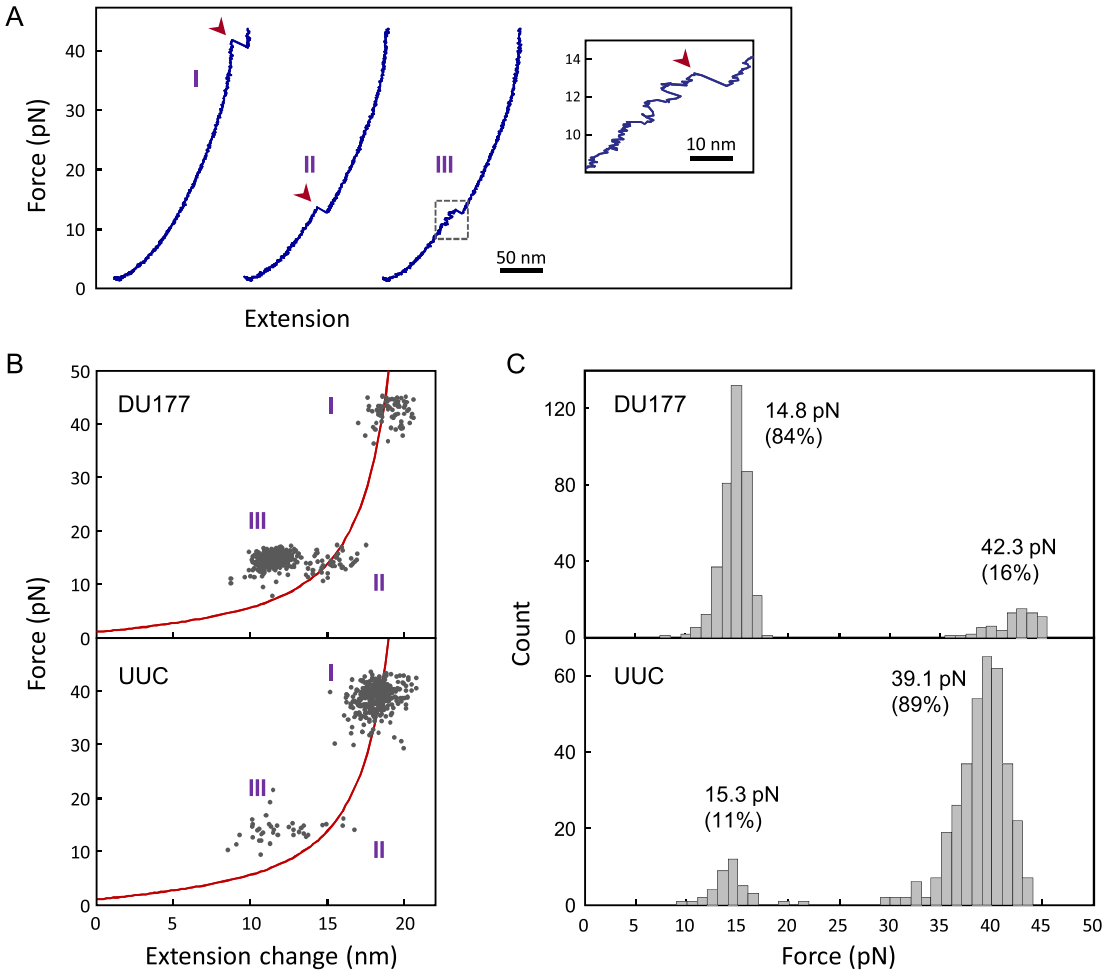

Figure 3. Experiments using optical tweezers to test regular pseudoknots. (**A**) Representative force-extension curves for DU177 in the process of gradually increasing the force, showing three major types of unfolding patterns (I, II and III). The structures usually disrupt suddenly and appear as a rip (transition) on the curve, indicated by arrowheads. Type III is featured with multiple back-and-forth small transitions before the rip (inset). (**B**) The unfolding forces and distance changes from all the transitions for DU177 (top) and the UUC mutant (bottom). The curves show the worm-like chain model for the native pseudoknot from DU177 or UUC, of which an unfolding transition is expected to be located on the curve. (**C**) Histograms of unfolding forces for DU177 (top) and UUC (bottom). The average force and population percentage (in parentheses) for the low-force peak and high-force peak are shown. See Supplementary Table S1 for more details.

Bimolecular RNA constructs to mimic a pseudoknot

As stem S1 of the pseudoknot is most likely the first target to be unwound by translocating ribosomes, measuring the unfolding force of the pseudoknot as a whole may not faithfully reflect the mechanical strength encountered by the ribosome. An ideal approach is to pull directly on stem S1 inside a pseudoknot; however, such an experimental design is technically challenging. Alternatively, we used the isolated S1-L1 hairpin of DU177, named DU177hp1 or hp1 for short, and annealed it with an 18-mer RNA oligomer (ss18) to mimic the pseudoknot conformation with the base-triple-mediated network (Figure 1B). Such bimolecular pseudoknots have been shown to preserve partial frameshift stimulation activity (36), indicating that at least some of the key structural features of a functional pseudoknot are maintained. The hairpin can be pulled directly in the presence of the RNA oligomer. Thus, the bimolecular design provides a convenient platform to assay the mechanical stability of stem S1 within the context of the pseudoknot.

When pulled by optical tweezers, hp1 alone experienced an unfolding force of 15.5 pN (Figure 4A). This value was equivalent to the low-force peak of DU177 unfolding (Figure 3C). When hp1 was annealed to ss11, an 11-mer RNA to reform stem S2 *in trans* (Figure 1B), the unfolding force was increased to 16.9 pN (Figure 4A). The enhanced stability likely resulted from the formation of the three major groove U•A*U base triples and the Hoogsteen A*U base pair at the helix junction. When the RNA oligomer was extended by two adenosines on the 5′ end (ss13) to potentially restore the two minor groove base triples (A•U*A and C•G*A), the unfolding force of the annealed hairpin was greatly increased to 21.0 pN (Figure 4A). The best stabilization of the hairpin was achieved at 22.3 pN, when all the missing nucleotides of loop L2 were added back to the RNA oligomer (ss18; Figure 4A). These results indicate that (i) base triples can be reestablished in the bimolecular mimic

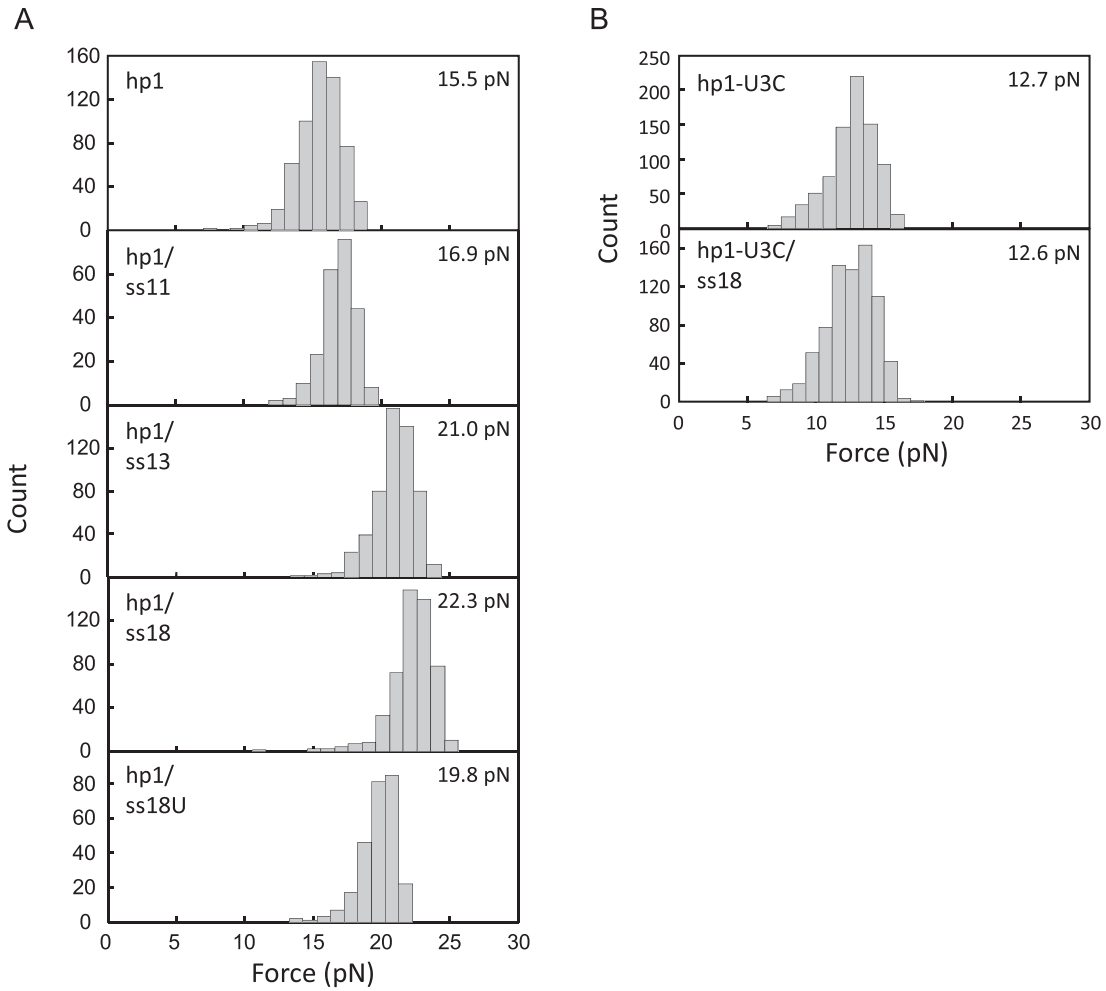

Figure 4. Distribution of unfolding forces for the bimolecular pseudoknots. (**A**) hp1 and (**B**) hp1-U3C, alone or annealed with the specified RNA oligomers to form bimolecular pseudoknots (see Figure 1B for illustrations), were pulled by optical tweezers for the measurements. The average force for each construct is shown on the top-right corner of each panel. See Supplementary Table S2 for more details.

and (ii) stem S1 can be stabilized by the loop L2 unpaired adenosine stretch acting *in trans*. The second point was confirmed by substituting U's for the A's in L2 (ss18U; Figure 1B). With the substitution, the unfolding force of the hairpin decreased by 2.5 pN from 22.3 to 19.8 pN (Figure 4A).

Role of the stem S2 base triples

To further probe the interaction between loop L2 and stem S1 of DU177, we applied smFRET to study the conformational dynamics of the hp1/ssRNA bimolecular pseudoknot. The 5′ and 3′ ends of ss18 were labeled with the fluorescent dyes Dy647 and Dy547, respectively. The labeled and annealed bimolecular pseudoknots were immobilized on the surface of a cover slip using a DNA strand complementary to the 5′ extension of hp1 (Figure 5A). FRET measurements were obtained by illuminating the samples with a 532 nm laser. The majority of FRET time traces were rather static (Supplementary Figure S3), suggesting no substantial conformational changes in the hp1/ss18 bimolecular pseudoknot. Figure 6A shows the FRET efficiency distribution from hundreds of molecules, which can be fit to a single Gaussian function centered at 0.65 (Figure 5 includes a summary of all the peak FRET values for better comparison among different constructs). To infer the loop L2 strand conformation in the bimolecular pseudoknot from the measured FRET efficiency, we synthesized a series of complementary ssDNA strands (dna9, dna10, dna12 and dna16) to form various lengths of duplexes with the dye-labeled ss18 (Figure 5B). The FRET efficiencies of these hybrids act as a primary reference to interpret the base pairing status of ss18 in the complex with hp1. As shown in Figures 5B and 6B, the FRET efficiencies of the hybrids decreased from 0.81 to 0.43 when the duplex length was increased from 9 to 16 bp. In this scenario, the conformation of ss18/hp1 (FRET = 0.65) was best approximated by that of ss18/dna12 (FRET = 0.68), in which 12 nt of ss18 were paired. This matches well to the known base-paired state of the native pseudoknot (Figure 1A; the same state is also depicted in Figure 5A for the bimolecular pseudoknot). Thus most, if not all, of the non-canonical base pairs of the DU177 pseudoknot are retained in the bimolecular pseudoknot. This is supported by the previous optical tweezers results, which showed that the unfolding force of hp1 increased in the pres-

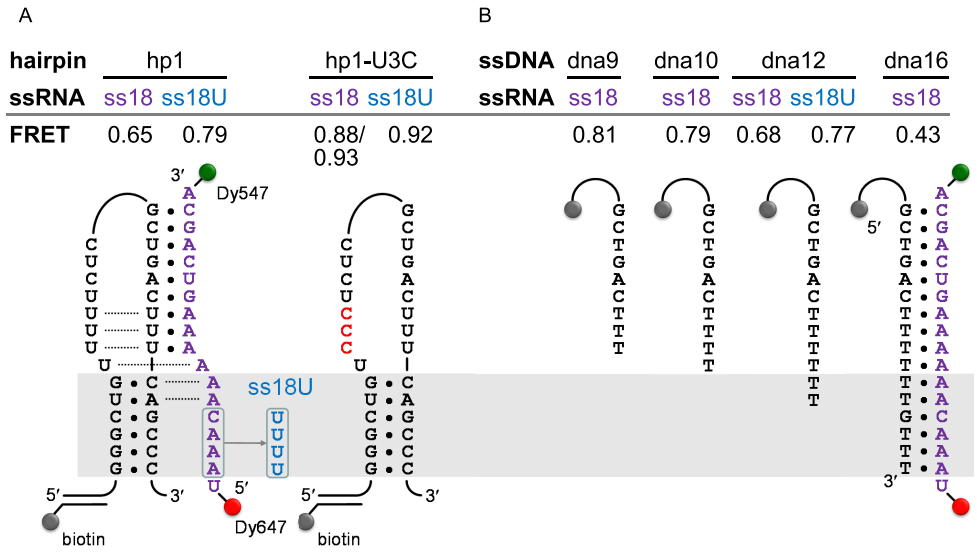

Figure 5. Design of and results from smFRET experiments. (**A**) Bimolecular pseudoknots constructed by annealing a hairpin (hp1 or hp1-U3C) to a single-stranded RNA (ssRNA; ss18 or ss18U). The 5′ and 3′ ends of the ssRNA were labeled with Dy647 and Dy547, respectively. A biotin-labeled DNA strand complementary to the 5′ overhang of the hairpin was used for immobilization. (**B**) DNA/RNA hybrids for control experiments. The dye-labeled ssRNA was annealed to a specified single-stranded DNA (ssDNA; dna9–dna16) containing a linker and a biotin tag on the 5′ end for immobilization. The measured FRET efficiency (see Figure 6) for each construct is summarized at the top. The gray shaded area highlights the corresponding stem S1 region for comparison among various constructs.

ence of the *trans*-acting RNA oligomers (Figure 4A). Moreover, when the 5′ overhang UAAAC of the ss18/dna12 hybrid was replaced by the all-pyrimidine sequence UUUUU (ss18U/dna12), the FRET efficiency increased from 0.68 to 0.77 (Figure 5B), indicating that the UAAAC overhang was dynamically constrained and thus the apparent distance between the two labeled dyes increased. This was probably a result of base stacking of the three consecutive adenosines. A similar FRET change was also observed for hp1 annealed with the same dye-labeled RNA oligomer (0.65 versus 0.79; Figure 5A). Taken together with the previous optical tweezers results, we conclude that the dynamically constrained adenosine stretch in the corresponding loop L2 region contributes significantly to the unwinding resistance of hp1 in the bimolecular pseudoknot.

Frameshift stimulation by bimolecular pseudoknots

By using two different single-molecule approaches, we have shown that both the conformation and stability of bimolecular pseudoknots were affected by the sequence and length of the annealed ssRNA oligomer. To determine if these variations also affected ribosomal frameshifting, we conducted *in vitro* translation assays using mRNA containing the hp1 hairpin to which the ss18* or ss18U* oligomer (equivalent to ss18 or ss18U, respectively; see Figure 1B) was presented for annealing. As shown in Figure 2B, the frameshifting efficiency increased in a dose-dependent manner, and ss18* was ∼2-fold as effective as ss18U* at the same concentrations. Thus, the adenosine stretch present in the annealed RNA oligomer not only increases the unwinding resistance of hp1 but also makes it a more potent frameshift stimulator.

Major groove base triples stabilize the other tertiary base pairs in the pseudoknot

Disrupting the major groove base triples (between stem S2 and loop L1) of DU177 decreases both the frameshifting efficiency and pseudoknot stability (13). This raises the question of whether the major groove base triples also influence the stabilization of stem S1 by the loop L2 strand, which in turn affects the frameshift stimulation. To test this, we constructed an hp1 mutant, hp1-U3C, which lacks the potential to form the three major groove U•A*U base triples in bimolecular pseudoknots (Figure 1B). In smFRET measurements, hp1-U3C/ss18 showed a high FRET value of 0.88–0.93 (Figure 5A), greater than that of hp1/ss18 (0.65). This value was even higher than that of the dna9/ss18 hybrid (0.81; Figure 5B), which mimics the conformation of ss18 in a structural framework containing the stem S2 only. Thus, the data indicate that the interaction between the 5′ side of ss18 and the stem of hp1-U3C was completely lost; the three adenosines (A6-A7-A8) of ss18, which otherwise were involved in the Hoogsteen base pair (U*A) and the two minor groove base triples (C•G*A and A•U*A), were released from base pairing. To confirm these results, we used optical tweezers to measure the mechanical stability of hp1-U3C. As shown in Figure 4B, the distributions of unfolding force of hp1-U3C were similar in the absence and presence of ss18, with an average of 12.7 and 12.6 pN, respectively. The lower unfolding force of hp1-U3C (compared to 15.5 pN for hp1) was probably due to the substitution of the weaker U*C for the stronger U*U base pairs in the loop region of the hairpin (45). Thus, all the tertiary base pair interactions, as well as the adenosine-stretch effect in the loop L2 region, occur only after the formation of the three major groove base triples in loop L1.

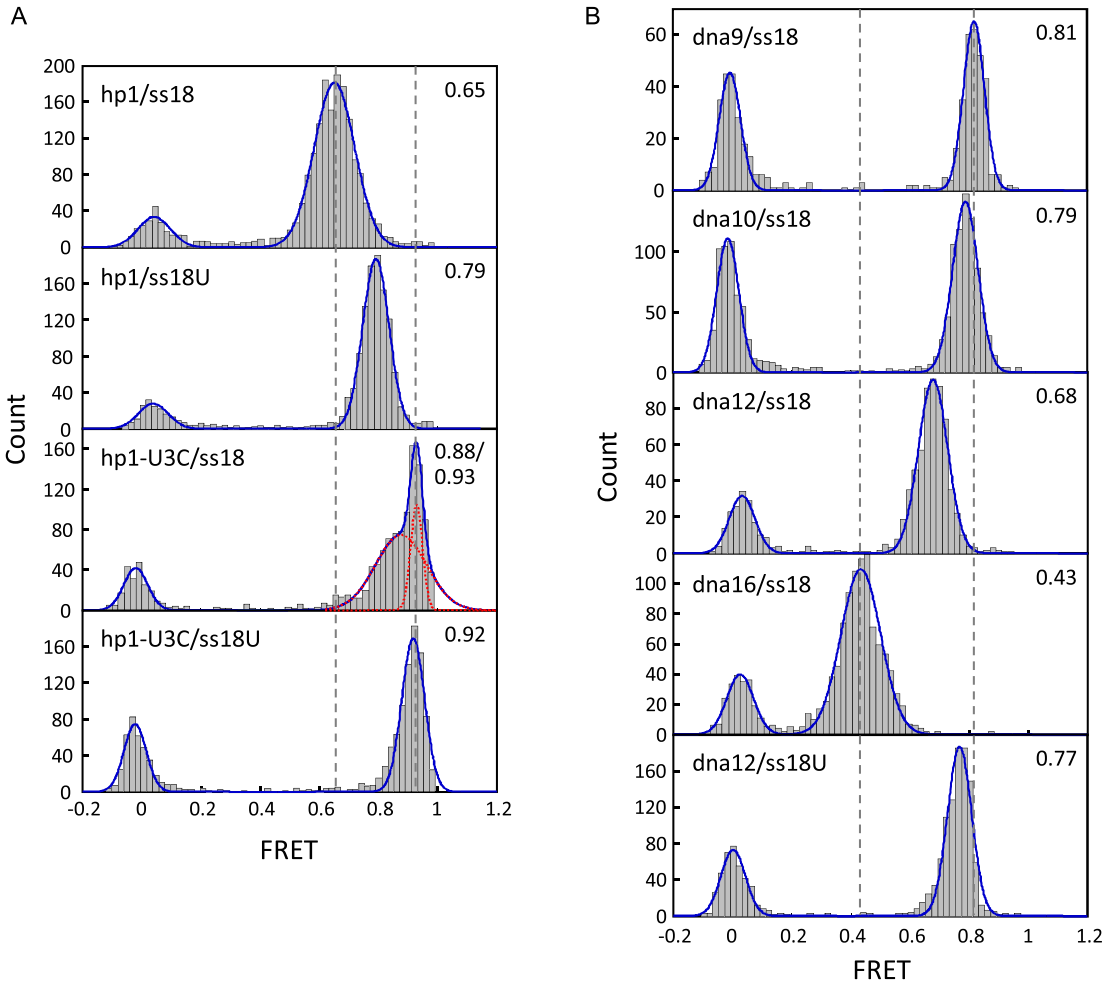

Figure 6. Distribution of FRET efficiency for (**A**) the bimolecular pseudoknots and (**B**) DNA/RNA hybrids (as described in Figure 5). The distributions can be fit to a single Gaussian function (solid curves) for all the constructs except for hp1-U3C/ss18, which is better fit to two functions (dotted curves) with the centers at 0.88 and 0.93. The fitted FRET values are shown on the top-right corner of each panel as well as in Figure 5. The FRET peak at 0 is attributed to the donor-only species.

DISCUSSION

In this study, we investigated both the folding and function of the loop L2 sequence in a native or bimolecular pseudoknot. The loop nucleotides align along the minor groove of the stem S1 helix to which the ribosome targets first and unwinds during translation. Thus, the loop sequence and its interaction with the stem may play a role in frameshift stimulation. We show that the presence of three consecutive adenosines (A167-A168-A169) on loop L2 of DU177 were important in increasing the efficiency of the pseudoknot as a frameshift stimulator (Figure 2). Single-molecule data further reveal that the sequence was dynamically constrained along stem S1, resulting in greater resistance of the stem to mechanical unwinding (Figures 4A and 5A). Consequently, we argue that the strengthened unwinding resistance of the stem is a major driving force to induce the ribosome to undergo frameshifting. According to the nuclear magnetic resonance (NMR) structure of DU177 (33,35), A167 and A168 stack consecutively, point to the minor groove of stem S1, and do not seem to form any hydrogen bonds with surrounding nucleotides (Figure 7A). By contrast, A169 swivels ∼90° away from the A167-A168 stack and locates so close to the G118•C96 base pair that two hydrogen bonds may potentially form, resulting in another putative base triple A169*G118•C96 (Supplementary Figure S4). Such structural features can explain the observed loop dynamic constraint. During translation, when the ribosome is about to unwind the right-handed stem S1 helix, the juxtaposed loop L2 nucleotides will rotate toward the proximal surface of the ribosome (Figure 7B) such that further unwinding/rotation may be blocked at some orientation; the bulky stacked adenines appear to have a better blocking effect. Alternatively, the constrained loop L2 may hinder the local twist of the helix by occupying its minor groove. Either of the two mechanisms can account for the contribution of the loop-enhanced helix unwinding resistance for efficient ribosomal frameshifting.

The bimolecular pseudoknot design allows for the direct pulling on the ribosome target duplex (hp1). This is a convenient approach to mimic and assess the action of ribosomes in a more realistic manner, as opposed to pulling on the whole native pseudoknot. The mechanical resis-

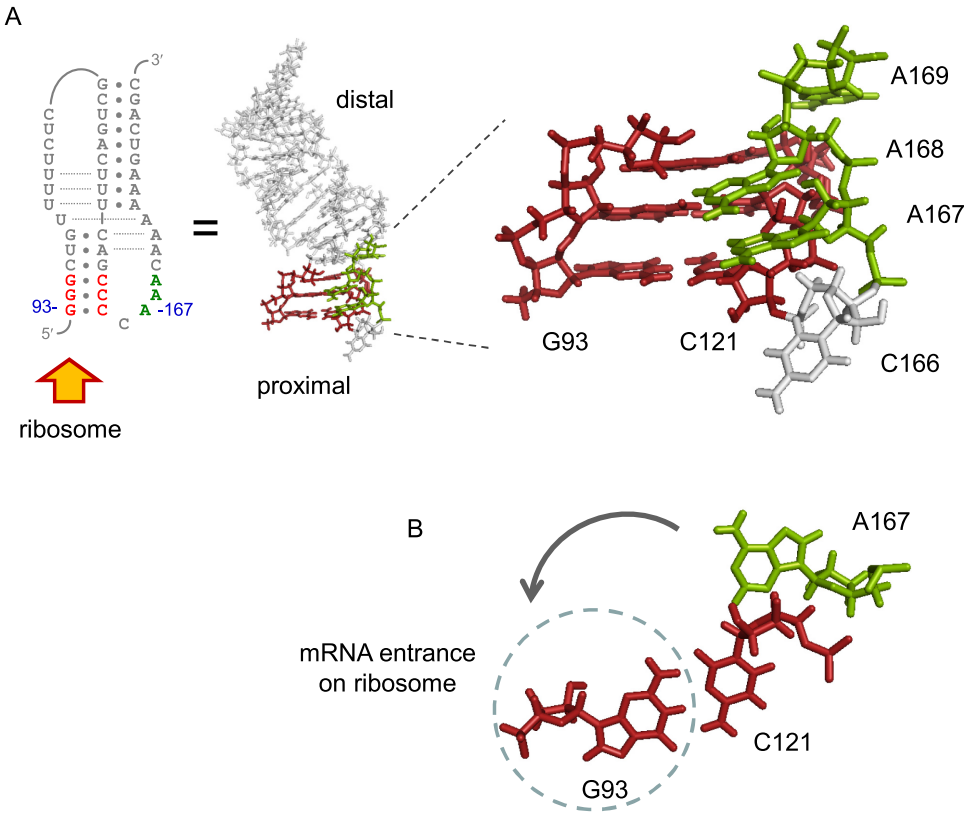

Figure 7. Conformation of the first ribosome target site on DU177. (**A**) The NMR structure (PDB ID: 2K96) and schematic drawing of DU177 are shown. The first three base pairs of stem S1 and the juxtaposed adenosine stretch in loop L2 are highlighted. A167 and A168 are base-stacked along the minor groove and do not form any hydrogen bonds with the surrounding residues. A169 swivels ∼90° away from the stack and may potentially form another base triple with G118•C96 (see Supplementary Figure S4). Secondary and tertiary base pairs in this region are expected to be targeted first by translocating ribosomes. Unwinding of the right-handed stem S1 helix will result in counterclockwise rotation of the whole structure, as viewed from the proximal end and illustrated in (**B**). Such motion can be hindered, otherwise the loop L2, including the adenosine stretch, may be deformed.

tance of hp1 was enhanced with the annealing of a single-stranded RNA, and the longer the RNA oligomers (from ss11 to ss18), the greater the unfolding force (Figure 4A). The results indicate that the tertiary base pairs between the hairpin and oligomers could be restored sequentially and additively. Viewed from the opening end of the hairpin, the restoration occurred from the distal major groove base triples (three of U•A*U, with ss11) to the minor groove base triples (C•G*A and A•U*A, with ss13), and to the proximal A167-A168-A169 effect (as discussed above, with ss18). Among all three types of tertiary base pair interactions, the distal major groove base triples can exist independently, whereas the other two could not form by themselves: when the major groove base triples were abolished, the stability of the hp1-U3C hairpin did not increase when annealed to the ss18 oligomer (Figure 4B). In other words, the three major groove base triples act as a core for the tertiary base pair interaction network inside the DU177 pseudoknot. Similarly, an NMR study for the murine leukemia virus pseudoknot revealed that formation of the base triple in the major groove of S2/L1 (distal) is responsible for the S1/L2 interactions (proximal) to cause ribosome read-through (46).

By studying a series of specialized RNA pseudoknots having different degrees of rotational freedom, Plant and Dinman proposed that ribosomal frameshifting is enhanced by the torsional resistance of the pseudoknots (47). RNA structures, called pseudo-pseudoknots, were made by annealing a complementary DNA strand to bridge the loop and downstream region of a hairpin derived from the L-A virus (47). The bridged region corresponded to a part of S2/L1 of the regular H-type pseudoknot and thus would be analogous to the major groove base triples in DU177. Recently, Dinman and colleagues further demonstrated that a pseudoknot from the human CCR5 mRNA could induce ∼10% of ribosomal frameshifting in HeLa cells, and the efficiency increased by a few folds when the distal stem S2 region of the pseudoknot was bound by a microRNA (48). These studies further underline the importance of the pseudoknot's distal tertiary base pair interactions in stimulating highly efficient ribosomal frameshifting. By contrast, pseudoknots from retroviruses or luteoviruses, including SRV-1 and BWYV, have a very short, usually 1 or 2 nt, loop L1 across the deep major groove of stem S2, whereas stem S1 and loop L2 are similar to DU177 in size and base composition (8,9,26,49) (see Supplementary Figure S1). The small loop L1 limits the extent of tertiary base pairs in the distal part of the pseudoknot and this may contribute, at least in part, to the relatively low frameshifting efficiencies of ∼20% for SRV-1 (50,51) and ∼10% for BWYV (52) as compared to the >50% of DU177 (13,36).

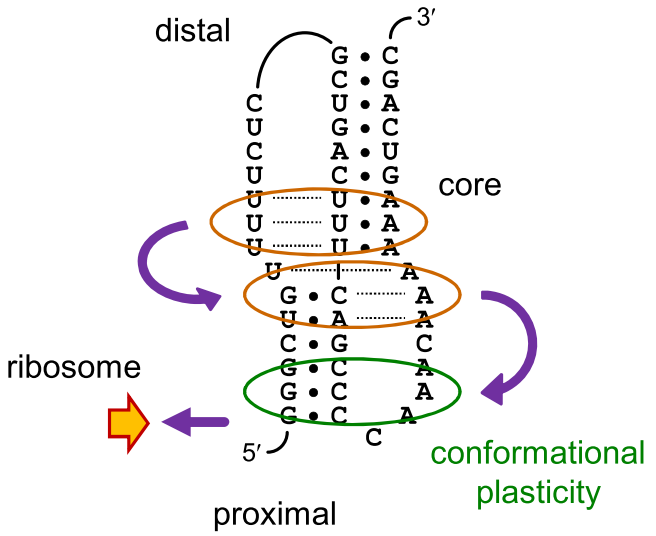

Figure 8. A model for the two-level brake mechanism. The three distal major groove base triples of the DU177 pseudoknot act as a core for the formation of other tertiary base pairs, including the loop-enhanced unwinding resistance of stem S1 at the proximal side (closest to translocating ribosomes). When the local conformation or stability of stem S1 is influenced by the ribosome, plasticity of the loop/stem interactions allows a conformational rearrangement in this region to re-establish the mechanical strength, given that the core tertiary base pairs retain. Thus the ribosome will encounter a persistent mechanical resistance during a finite translocating process.

Chen *et al*. showed that the frameshifting efficiency was positively correlated with pseudoknot mechanical stability, based on the study of a series of DU177 mutants, of which various base triples were disrupted (13). Subsequently, Ritchie *et al*. found that such a correlation did not exist for another set of RNA pseudoknots derived from different viruses (14). Here, we also observed a weak correlation for the UUC mutant of DU177; the mutation in loop L2 decreased the frameshifting efficiency of UUC by 62%, but its mechanical stability decreased only 8% (Figures 2A and 3C). We reconcile the seemingly contradictory observations in the following manner. In its basic form, a pseudoknot consists of three strands running back and forth. The triplex is held together by stems (binding two strands) and base triples (binding all the three strands) in DU177 and many viral RNA pseudoknots. The force is mainly exerted along the axis of the triplex when pulled by optical tweezers. Disrupting the base triple interactions (as in the experiments by Chen *et al*.) can have 2-fold outcomes. First, the shearing resistance, and thus the overall mechanical stability, of the triplex is effectively reduced. Second, due to the folding dependence of various tertiary base pair interactions observed in DU177, the loop-enhanced unwinding resistance of stem S1 is attenuated, resulting in a decrease of frameshifting efficiency. These two correlated outcomes in the base triple mutants of DU177 are not necessarily applicable to the loop mutant UUC or to pseudoknots having various sizes and folding topologies (as in the experiments by Ritchie *et al*.). The sequence change in loop L2 of the UUC mutant would minimally affect the triplex shearing but greatly impact the local helix unwinding, and thus the results did not fit with the prediction of Chen *et al*. Interestingly, when using optical tweezers, we observed a substantial decrease in the population of the folding intermediates, from 84% in DU177 to 11% in UUC (Figure 3C). This is consistent with the model by Ritchie *et al*., whereby the frameshifting efficiency correlates with the pseudoknot conformational plasticity, thus having more intermediate structures (14). While the features of conformational plasticity have been extensively discussed (14), our current findings bring to light the following: when a portion of the proximal tertiary base pair interactions (such as the one between the adenosine stretch and stem S1) of the pseudoknot is disrupted by translocating ribosomes, a rearrangement of nucleotide interactions in this region is possible to reestablish a comparable resistance to the ribosome, given that the distal tertiary base pairs (such as the major groove base triples) can still be retained by themselves, as in the case of DU177.

Finally, we propose a two-level brake mechanism to explain the mechanical reaction of an RNA pseudoknot targeted by ribosomes, with the reaction in turn determining the frameshifting efficiency (Figure 8). Firstly, the loop L2 adenosine stretch enhances the unwinding resistance of stem S1, providing the first brake level to the translocating ribosome as soon as it encounters the RNA pseudoknot. The folding of the pseudoknot can be maintained even if the first few base pairs of stem S1 are opened. This is because the distal tertiary base pairs still exist and can act as a core, initiating a conformational rearrangement of the proximal secondary/tertiary structures to reach a thermodynamically stable state. This provides the second brake level and thus a persistent mechanical strength to the ribosome. As discussed above, the second brake level can serve as another suitable molecular explanation to the 'pseudoknot conformational plasticity' (14).

SUPPLEMENTARY DATA

Supplementary Data are available at NAR Online.

ACKNOWLEDGEMENTS

We thank Dr Tae-Young Yoon and his group at Yonsei University (then at KAIST), Republic of Korea, for their kind assistance in setting up the smFRET system.

FUNDING

Ministry of Science and Technology [101-2628-B-002-001-MY4, 103-2627-M-002-001 to J.-D.W.; 103-2627-M-005-001 to K.-Y.C.]; National Taiwan University [NTU-CDP-104R7749 to J.-D.W]. Funding for open access charge: Ministry of Science and Technology [105-2311-B-002-038].
Conflict of interest statement. None declared.

REFERENCES

1. Baranov,P.V., Gesteland,R.F. and Atkins,J.F. (2002) Recoding: translational bifurcations in gene expression. *Gene*, **286**, 187–201.
2. Dinman,J.D. (2012) Mechanisms and implications of programmed translational frameshifting. *Wiley Interdiscip. Rev. RNA*, **3**, 661–673.
3. Farabaugh,P.J. (1996) Programmed translational frameshifting. *Microbiol. Rev.*, **60**, 103–134.

4. Atkins,J.F., Loughran,G., Bhatt,P.R., Firth,A.E. and Baranov,P.V. (2016) Ribosomal frameshifting and transcriptional slippage: From genetic steganography and cryptography to adventitious use. *Nucleic Acids Res.*, **44**, 7007–7078.
5. Brierley,I., Jenner,A.J. and Inglis,S.C. (1992) Mutational analysis of the 'slippery-sequence' component of a coronavirus ribosomal frameshifting signal. *J. Mol. Biol.*, **227**, 463–479.
6. Dinman,J.D., Icho,T. and Wickner,R.B. (1991) A -1 ribosomal frameshift in a double-stranded RNA virus of yeast forms a gag-pol fusion protein. *Proc. Natl. Acad. Sci. U.S.A.*, **88**, 174–178.
7. ten Dam,E.B., Pleij,C.W. and Bosch,L. (1990) RNA pseudoknots: translational frameshifting and readthrough on viral RNAs. *Virus Genes*, **4**, 121–136.
8. Giedroc,D.P., Theimer,C.A. and Nixon,P.L. (2000) Structure, stability and function of RNA pseudoknots involved in stimulating ribosomal frameshifting. *J. Mol. Biol.*, **298**, 167–185.
9. Giedroc,D.P. and Cornish,P.V. (2009) Frameshifting RNA pseudoknots: structure and mechanism. *Virus Res.*, **139**, 193–208.
10. Staple,D.W. and Butcher,S.E. (2005) Solution structure and thermodynamic investigation of the HIV-1 frameshift inducing element. *J. Mol. Biol.*, **349**, 1011–1023.
11. Namy,O., Moran,S.J., Stuart,D.I., Gilbert,R.J. and Brierley,I. (2006) A mechanical explanation of RNA pseudoknot function in programmed ribosomal frameshifting. *Nature*, **441**, 244–247.
12. Brierley,I., Gilbert,R.J.C. and Pennell,S. (2010) Pseudoknot-Dependent Programmed -1 Ribosomal Frameshifting: Structures, Mechanisms and Models. In: Atkins,JF and Gesteland,RF (eds). *Recoding: Expansion of Decoding Rules Enriches Gene Expression*. Springer, NY, Vol. **24**, pp. 149–174.
13. Chen,G., Chang,K.Y., Chou,M.Y., Bustamante,C. and Tinoco,I. Jr (2009) Triplex structures in an RNA pseudoknot enhance mechanical stability and increase efficiency of -1 ribosomal frameshifting. *Proc. Natl. Acad. Sci. U.S.A.*, **106**, 12706–12711.
14. Ritchie,D.B., Foster,D.A. and Woodside,M.T. (2012) Programmed -1 frameshifting efficiency correlates with RNA pseudoknot conformational plasticity, not resistance to mechanical unfolding. *Proc. Natl. Acad. Sci. U.S.A.*, **109**, 16167–16172.
15. Bidou,L., Stahl,G., Grima,B., Liu,H., Cassan,M. and Rousset,J.P. (1997) In vivo HIV-1 frameshifting efficiency is directly related to the stability of the stem-loop stimulatory signal. *RNA*, **3**, 1153–1158.
16. Mouzakis,K.D., Lang,A.L., Vander Meulen,K.A., Easterday,P.D. and Butcher,S.E. (2013) HIV-1 frameshift efficiency is primarily determined by the stability of base pairs positioned at the mRNA entrance channel of the ribosome. *Nucleic Acids Res.*, **41**, 1901–1913.
17. Zhong,Z., Yang,L., Zhang,H., Shi,J., Vandana,J.J., Lam,D.T., Olsthoorn,R.C., Lu,L. and Chen,G. (2016) Mechanical unfolding kinetics of the SRV-1 gag-pro mRNA pseudoknot: possible implications for -1 ribosomal frameshifting stimulation. *Sci. Rep.*, **6**, 39549.
18. Takyar,S., Hickerson,R.P. and Noller,H.F. (2005) mRNA helicase activity of the ribosome. *Cell*, **120**, 49–58.
19. Qu,X., Wen,J.-D., Lancaster,L., Noller,H.F., Bustamante,C. and Tinoco,I. Jr (2011) The ribosome uses two active mechanisms to unwind messenger RNA during translation. *Nature*, **475**, 118–121.
20. Wen,J.-D., Lancaster,L., Hodges,C., Zeri,A.C., Yoshimura,S.H., Noller,H.F., Bustamante,C. and Tinoco,I. Jr (2008) Following translation by single ribosomes one codon at a time. *Nature*, **452**, 598–603.
21. Brierley,I., Pennell,S. and Gilbert,R.J. (2007) Viral RNA pseudoknots: versatile motifs in gene expression and replication. *Nat. Rev. Microbiol.*, **5**, 598–610.
22. Mazauric,M.H., Leroy,J.L., Visscher,K., Yoshizawa,S. and Fourmy,D. (2009) Footprinting analysis of BWYV pseudoknot-ribosome complexes. *RNA*, **15**, 1775–1786.
23. Egli,M., Minasov,G., Su,L. and Rich,A. (2002) Metal ions and flexibility in a viral RNA pseudoknot at atomic resolution. *Proc. Natl. Acad. Sci. U.S.A.*, **99**, 4302–4307.
24. Pallan,P.S., Marshall,W.S., Harp,J., Jewett,F.C. 3rd, Wawrzak,Z., Brown,B.A. 2nd, Rich,A. and Egli,M. (2005) Crystal structure of a luteoviral RNA pseudoknot and model for a minimal ribosomal frameshifting motif. *Biochemistry*, **44**, 11315–11322.
25. Cornish,P.V., Hennig,M. and Giedroc,D.P. (2005) A loop 2 cytidine-stem 1 minor groove interaction as a positive determinant for pseudoknot-stimulated -1 ribosomal frameshifting. *Proc. Natl. Acad. Sci. U.S.A.*, **102**, 12694–12699.
26. Michiels,P.J., Versleijen,A.A., Verlaan,P.W., Pleij,C.W., Hilbers,C.W. and Heus,H.A. (2001) Solution structure of the pseudoknot of SRV-1 RNA, involved in ribosomal frameshifting. *J. Mol. Biol.*, **310**, 1109–1123.
27. Chamorro,M., Parkin,N. and Varmus,H.E. (1992) An RNA pseudoknot and an optimal heptameric shift site are required for highly efficient ribosomal frameshifting on a retroviral messenger RNA. *Proc. Natl. Acad. Sci. U.S.A.*, **89**, 713–717.
28. Shen,L.X. and Tinoco,I. Jr (1995) The structure of an RNA pseudoknot that causes efficient frameshifting in mouse mammary tumor virus. *J. Mol. Biol.*, **247**, 963–978.
29. Wang,Y., Wills,N.M., Du,Z., Rangan,A., Atkins,J.F., Gesteland,R.F. and Hoffman,D.W. (2002) Comparative studies of frameshifting and nonframeshifting RNA pseudoknots: a mutational and NMR investigation of pseudoknots derived from the bacteriophage T2 gene 32 mRNA and the retroviral gag-pro frameshift site. *RNA*, **8**, 981–996.
30. Olsthoorn,R.C., Reumerman,R., Hilbers,C.W., Pleij,C.W. and Heus,H.A. (2010) Functional analysis of the SRV-1 RNA frameshifting pseudoknot. *Nucleic Acids Res.*, **38**, 7665–7672.
31. Holland,J.A., Hansen,M.R., Du,Z. and Hoffman,D.W. (1999) An examination of coaxial stacking of helical stems in a pseudoknot motif: the gene 32 messenger RNA pseudoknot of bacteriophage T2. *RNA*, **5**, 257–271.
32. Moffitt,J.R., Chemla,Y.R., Smith,S.B. and Bustamante,C. (2008) Recent advances in optical tweezers. *Annu. Rev. Biochem.*, **77**, 205–228.
33. Theimer,C.A., Blois,C.A. and Feigon,J. (2005) Structure of the human telomerase RNA pseudoknot reveals conserved tertiary interactions essential for function. *Mol. Cell*, **17**, 671–682.
34. Theimer,C.A., Finger,L.D., Trantirek,L. and Feigon,J. (2003) Mutations linked to dyskeratosis congenita cause changes in the structural equilibrium in telomerase RNA. *Proc. Natl. Acad. Sci. U.S.A.*, **100**, 449–454.
35. Kim,N.K., Zhang,Q., Zhou,J., Theimer,C.A., Peterson,R.D. and Feigon,J. (2008) Solution structure and dynamics of the wild-type pseudoknot of human telomerase RNA. *J. Mol. Biol.*, **384**, 1249–1261.
36. Chou,M.Y. and Chang,K.Y. (2010) An intermolecular RNA triplex provides insight into structural determinants for the pseudoknot stimulator of -1 ribosomal frameshifting. *Nucleic Acids Res.*, **38**, 1676–1685.
37. Ritchie,D.B., Soong,J., Sikkema,W.K. and Woodside,M.T. (2014) Anti-frameshifting ligand reduces the conformational plasticity of the SARS virus pseudoknot. *J. Am. Chem. Soc.*, **136**, 2196–2199.
38. Joo,C., Balci,H., Ishitsuka,Y., Buranachai,C. and Ha,T. (2008) Advances in single-molecule fluorescence methods for molecular biology. *Annu. Rev. Biochem.*, **77**, 51–76.
39. Grentzmann,G., Ingram,J.A., Kelly,P.J., Gesteland,R.F. and Atkins,J.F. (1998) A dual-luciferase reporter system for studying recoding signals. *RNA*, **4**, 479–486.
40. Wen,J.-D., Manosas,M., Li,P.T., Smith,S.B., Bustamante,C., Ritort,F. and Tinoco,I. Jr (2007) Force unfolding kinetics of RNA using optical tweezers. I. Effects of experimental variables on measured results. *Biophys. J.*, **92**, 2996–3009.
41. Wu,Y.-J., Wu,C.-H., Yeh,A.Y.-C. and Wen,J.-D. (2014) Folding a stable RNA pseudoknot through rearrangement of two hairpin structures. *Nucleic Acids Res.*, **42**, 4505–4515.
42. Bustamante,C., Marko,J.F., Siggia,E.D. and Smith,S. (1994) Entropic elasticity of lambda-phage DNA. *Science*, **265**, 1599–1600.
43. Aitken,C.E., Marshall,R.A. and Puglisi,J.D. (2008) An oxygen scavenging system for improvement of dye stability in single-molecule fluorescence experiments. *Biophys. J.*, **94**, 1826–1835.
44. Lee,H.W., Ryu,J.Y., Yoo,J., Choi,B., Kim,K. and Yoon,T.Y. (2013) Real-time single-molecule coimmunoprecipitation of weak protein-protein interactions. *Nat. Protoc.*, **8**, 2045–2060.
45. Zhong,Z., Soh,L.H., Lim,M.H. and Chen,G. (2015) A U·U pair-to-U·C pair mutation-induced RNA native structure destabilisation and stretching-force-induced RNA misfolding. *Chempluschem*, **80**, 1267–1278.
46. Houck-Loomis,B., Durney,M.A., Salguero,C., Shankar,N., Nagle,J.M., Goff,S.P. and D'Souza,V.M. (2011) An

equilibrium-dependent retroviral mRNA switch regulates translational recoding. *Nature*, **480**, 561–564.
47. Plant,E.P. and Dinman,J.D. (2005) Torsional restraint: a new twist on frameshifting pseudoknots. *Nucleic Acids Res.*, **33**, 1825–1833.
48. Belew,A.T., Meskauskas,A., Musalgaonkar,S., Advani,V.M., Sulima,S.O., Kasprzak,W.K., Shapiro,B.A. and Dinman,J.D. (2014) Ribosomal frameshifting in the CCR5 mRNA is regulated by miRNAs and the NMD pathway. *Nature*, **512**, 265–269.
49. Su,L., Chen,L., Egli,M., Berger,J.M. and Rich,A. (1999) Minor groove RNA triplex in the crystal structure of a ribosomal frameshifting viral pseudoknot. *Nat. Struct. Biol.*, **6**, 285–292.
50. ten Dam,E., Brierley,I., Inglis,S. and Pleij,C. (1994) Identification and analysis of the pseudoknot-containing gag-pro ribosomal frameshift signal of simian retrovirus-1. *Nucleic Acids Res.*, **22**, 2304–2310.
51. ten Dam,E.B., Verlaan,P.W. and Pleij,C.W. (1995) Analysis of the role of the pseudoknot component in the SRV-1 gag-pro ribosomal frameshift signal: loop lengths and stability of the stem regions. *RNA*, **1**, 146–154.
52. Kim,Y.G., Su,L., Maas,S., O'Neill,A. and Rich,A. (1999) Specific mutations in a viral RNA pseudoknot drastically change ribosomal frameshifting efficiency. *Proc. Natl. Acad. Sci. U.S.A.*, **96**, 14234–14239.